Geopersia 2021, 11(1): 101-114
DOI: 10.22059/GEOPE.2020.297014.648530

RESEARCH PAPER

Influence of mechanical parameters and overburden pressure on the mechanical evolution of fault propagation folds: insights from 2D finite-element elastic-plastic models applied to the Ayegan anticline, central Alborz

Anis Khalife- Soltani [1], Seyed Ahmad Alavi [1,*], Mohammad R. Ghassemi [2, 3], Seyed Mehdi Ganjiani [4]

[1] Department of sedimentary and oil basins, Faculty of Earth Sciences, Shahid Beheshti University, Tehran, Iran
[2] Research Institute for Earth Sciences, Geological Survey of Iran, Tehran, Iran
[3] School of Geology, College of Science, University of Tehran, Tehran, Iran
[4] Department of Mechanical Engineering, University of Tehran, Tehran, Iran

Received: 01 February 2020, Revised: 04 July 2020, Accepted: 28 July 2020

Abstract
Fault-related folding, due to the variety of tectonic setting, seismic and economic importance, has always been of interest to geologists. In this study, we investigate the influence of different aspects of the mechanical parameters (Young's modulus, Poisson's ratio, dilation angle, and cohesion) and boundary conditions (overburden pressure) to determine the fault-propagation folding style and its mechanical evolution through the use of a series of 2D finite-element elastic-plastic models so that the use of inelastic relationships allows permanent strains to develop in response to the applied loads. All FE-models with the mechanical parameters reduced to 15%, except for Young's modulus and overburden pressure, lead to lower half- wavelength and amplitude values concerning the reference model, and as these parameters are changed by 15% and 30% simultaneously to validate the results, the area reduction is dramatically increased. FE-model results show that area changes in fault propagation fold are as a function of mechanical stratigraphy, mechanical parameters, and overburden pressure. Area loss can also lead to a decrease in permeability through intergranular mechanisms. We apply these insights to the Ayegan anticline, central Alborz that generally show well-designed FE-modelling matched overall structural geometry in the kink-style kinematic model.

Keywords: Fault- Propagation Fold, Mechanical parameters, Finite-element method, Ayegan nticline, Central Alborz

Introduction

Fault-related folds observe in the various tectonic settings in both compressional and extensional regimes (e.g., Ferrill et al., 2012; Brandes & Tanner, 2014). Fault-related folds have always been of interest to geologists because of their economic and seismic importance (e.g. Johnson & Segall, 2004; Guzofski et al., 2007; Lin et al., 2007; DeVecchio et al., 2012). Fault-propagation folds are an important type of fault-related folds that form as a consequence of variations in the slip along the fault as fault propagates upward so that they slip on a fault decrease to zero at the tip. Fault-propagation folds tend to have long, gently-dipping backlimbs, steep and narrow forelimbs, and an active locus of folding in the syncline associated with the

* Corresponding author e-mail: a-alavi@sbu.ac.ir

propagating fault tip (Suppe & Medwedeff, 1990; Hughes et al., 2014; Hughes & Shaw, 2015). Early concepts of fault-propagation folds were developed into several geometric and kinematic models (e.g., Suppe, 1983; Mitra, 1990; Suppe & Medwedeff, 1990; Brandes & Tanner, 2014). Thereafter, studies on fault- propagation folds (both extensional and contractional regimes) have been widely extended and successfully analyzed using field and subsurface seismic reflection data (e.g., Mitra, 1990; Suppe & Medwedeff, 1990; Alipoor et al., 2019; Derikvand et al., 2018, 2019), analog sandbox (e.g., McClay, 1995; Bernand et al., 2007), and numerical models (e.g., Albertz & Lingery, 2012; Albertz & Sans, 2012; Jabbour et al, 2012; Hunghes & Show, 2015; Thebian et al, 2017).

Understanding the circumstances that favor the development of specific structural styles is relevant to several applications such as regional tectonic studies. Different styles feature different relationships between the amount of shortening, amount of uplift, the role of mechanical stratigraphy, the role of the underlying structural inheritance, that are associated with their formation; thus, proper identification and interpretation of the structural evolution and structural style are essential to constructing the accurate understanding of the surface and subsurface geometry of structures. In this regard, numerical modeling using methods such as finite element (FE), boundary element, and discrete element provides tools for simulating and tracking the temporal and spatial evolution of stress distribution, characteristic and sequential evolution of structures, strain localization the prediction of onset of associated geological structures at different scales. (e.g., Smart et al., 2012b; Hughes et al., 2014; Maerten et al., 2014; Hughes & Shaw, 2015; Nabavi et al., 2017, 2018a, 2018b, 2020; Cruz et al., 2019).

To investigate shape changes of fault-propagation folds with respect to the geometric parameters, and also mechanical evolution of them, including strain localization, we utilize results from 2D static numerical FE-models using ABAQUS^{TM} software package. This study seeks to address the importance and influence of (1) mechanical parameters, including Young's modulus, Poisson's ratio, dilation angle, and cohesion, and (2) overburden pressure, on the structural and mechanical evolution of fault-propagation folds in contractional settings. The outcome of this study is compared to the Ayegan anticline in the central Alborz, which is suitable, but rather little-studied, an example of a fault-propagation fold. Furthermore, numerical results are discussed with respect to earlier mechanical modeling studies.

Geological and tectonic setting

With an approximate length and width of respectively 600 and 100 km, the Alborz Mountains Range are located in the north of Iran and to the south of the Caspian Sea (Allen et al., 2003; Vernant et al., 2004). The Alborz Mountains Range form part of the Alpine-Himalayan orogenic belt in western Asia (Alavi, 1996) in the actively deforming Arabian and Eurasian plates collision zone from the Cenozoic and pervasive intracontinental deformation with exhumation pulses (Allen et al., 2003; Ballato et al., 2011, 2013) with the convergence rate of 22 mm/yr, resulting in an NNE-SSW oriented shortening of the crust (Vernant et al., 2004; Guest et al., 2006b). Alborz Mountains have a general East-West trend, a clear V-shaped convexity toward the south (Stocklin, 1968), and is divided into western, central, and eastern parts.

The belt was affected by polyphase deformation, from the Eo-Cimmerian orogeny to late Tertiary-Quaternary intracontinental transpressional deformation that is accommodated oblique convergence along several oblique-reverse faults such as Mosh and Taleghan faults (Vernant et al., 2004; Landgraf et al., 2009; Zanchi et al., 2009; Ballato et al., 2013; Nabavi et al., 2017). The study area is located in the central Alborz (Fig. 1). In the central Alborz, the Caspian, North Alborz, Kandovan, Taleghan, Mosha and the North Tehran faults are the major features extensively studied over the past decade (Ehteshami Moinabadi & Yassaghi, 2007, Yassaghi & Madanipour, 2008, Yassaghi & Naeimi, 2011, Ballato et al., 2013, Ghassemi et al., 2014).

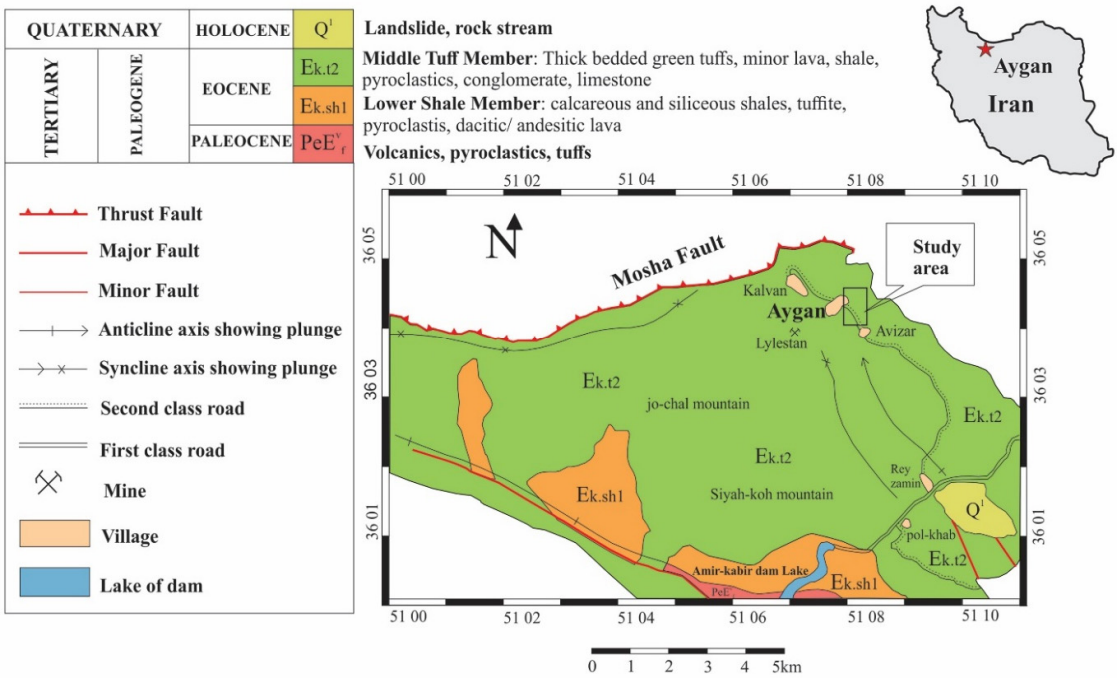

Figure 1. Simplified geological-structural map of the Ayegan area. The approximate location of the study site is marked by a rectangle

In Paleozoic time, sedimentary gaps are typical for the Alborz belt due to epirogenic movements. In addition, as a result of Late Cretaceous epirogenic movements, major uplift took place in the central Alborz (Yassaghi & Naeimi, 2011, Ballato et al., 2013). The first and second contractional phases in the central Alborz took place during the Oligocene, and Miocene-Pliocene times, respectively, which are accompanied by folding, faulting, fault reactivation, and folding axis deviations. The central Alborz has experienced extensive multiphase kinematic reversal brittle and ductile event during the Oligocene-Miocene convergence event (Allen et al., 2003; Zanchi et al., 2009; Ehteshami-Moinabadi & Yassaghi, 2007; Yassaghi & Madanipour, 2008; Yassaghi & Naeimi, 2011; Ballato et al., 2011). Inversions of major pre-existing faults, the Mosha faults for example which are the most outstanding structure in the southern part of the central Alborz , and also fault-controlled sub-basins like the Karaj basin led to the formation of fault-related folds and a positive flower-shaped structural framework of the central Alborz range (Zanchi et al., 2009; Ehteshami-Moinabadi & et al., 2012; Ehteshami-Moinabadi & Yassaghi, 2013).

The Ayegan anticline has been investigated as an asymmetric contractional fault-propagation fold in Eocene tuffite and shale layers of the Karaj Formation that verged toward the southeast. The Ayegan anticline arises from the operation of the footwall short-cut thrust branching from the Mosha fault during basin inversion in the Oligocene-Miocene contractional event (Ehteshami-Moinabadi & Yassaghi, 2007).

Model setup

A series of 2D plane strain, static, and elastic-plastic behavior is adopted for FE-modelling of fault-propagation folds and the Ayegan anticline using ABAQUS^{TM} software version 2017. The initial FE-model geometry was based on the restored cross-section constrained by field photographs, and incorporate the generalized mechanical stratigraphy for the study structure.

The elastic portion of the material model contains two elastic constants such as Young's modulus and Poisson's ratio, that relate stress and strain associated with a two-dimensional

plane strain relationship simplified form of Hooke's Law (Smart et al., 2012b):

$$\begin{Bmatrix} \sigma_{xx} \\ \sigma_{yy} \\ \sigma_{xy} \end{Bmatrix} = \frac{E}{(1+\nu)(1-2\nu)} \begin{bmatrix} 1-\nu & \nu & 0 \\ \nu & 1-\nu & 0 \\ 0 & 0 & 1-2\nu \end{bmatrix} \begin{Bmatrix} \varepsilon_{xx} \\ \varepsilon_{yy} \\ \varepsilon_{xy} \end{Bmatrix} \quad (1)$$

where E is Young's modulus and ν is Poisson's ratio. The plastic portion of the material model is the standard Mohr-Coulomb formulation (Smart et al., 2012b):

$$F = R_{mc}q - p\tan\varphi - C_0 \quad \begin{cases} F<0 & Elastic \\ F=0 & Plastic \end{cases} \quad (2)$$

Where F is a yield function that controls the onset of plastic behavior, p is the equivalent pressure or mean stress, q is the Mises equivalent stress, C0 is the cohesion, φ is the friction angle, and Rmc is the Mohr-Coulomb deviatoric stress measure (Smart et al., 2012b). All material and mechanical properties used for the FE-models are listed in Table. 1.

The initial 2D FE-model geometries of the Ayegan anticline were based on the restored geological cross-section constrained by field observations and photographs, topographic data, Google Earth images, and integrate the generalized mechanical stratigraphy in the study area and anticline (Figs 2, 3). The final (i.e., arc length) and initial (i.e., unfolded state) length of the Ayegan anticline are estimated 517 m and 817 m, respectively, using MoveTM software. Hence, the amount of shortening is 300 m or 37%. The Ayegan anticline and study FE-model contain 9 layers in four different mechanical properties (Fig. 3, Table. 1). Rheology and thickness of layers are marked in Figure 3.

Table 1. Materials Property used in finite element models

Layer	lithology	ρ	E	ν	φ	ψ	C_0
5-9	Limestone	3000	37	0.3	32	16	35
3-4	Marl-limestone	2900	41	0.3	32	16	30
2	Marl	2700	11.5	0.35	28	14	9.5
1	Tuff	2500	11.5	0.31	40	20	20.7

ρ= density (kg/m^3); E = Young's Modulus (GPa); ν = Poisson's Ratio;φ = Friction Angle (°); ψ = Dilation Angle (°); C_0 = Cohesion (MPa).

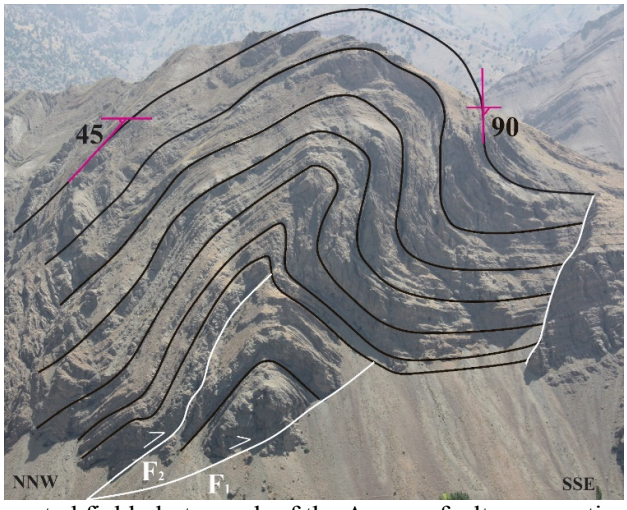

Figure 2. Interpreted field photograph of the Ayegan fault-propagation fold structure

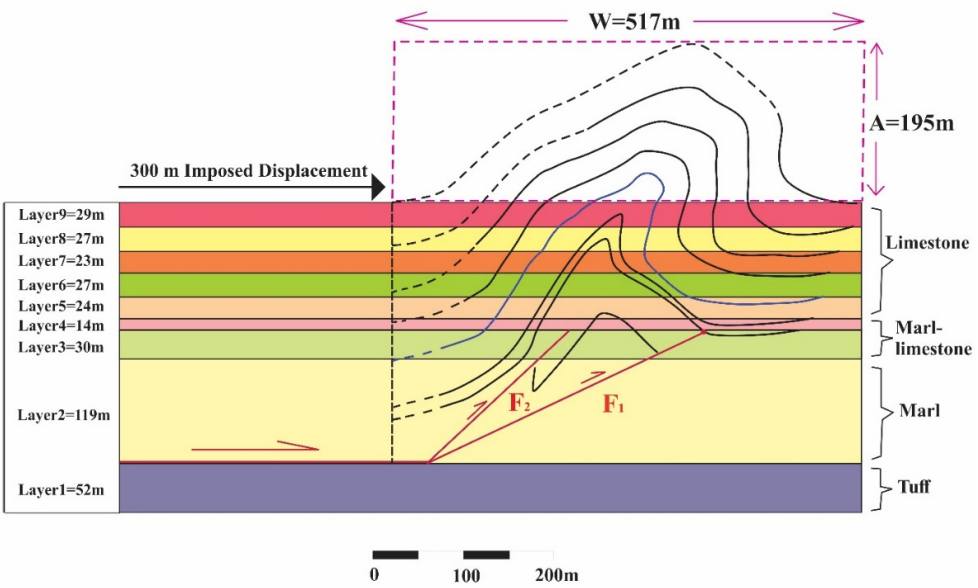

Figure 3. Geological cross-section and restoration of the deformed section of the Ayegan fault-propagation fold to initial undeformed geometry that contains 9 mechanical layers with a lower detachment at the base of the structure and two pre-existing thrust faults (F1 and F2). Half-wavelength and the amplitude of the fold structure are marked by 'W' and 'A', respectively. Eroded and/or covered parts of the structure are marked in black dashed lines. This section used in order to the finite element model configuration

Moreover, this study presents the results of FE-models of fault-propagation folds developed over two pre-existing inclined reverse faults F_1 and F_2 of different dips (Fig. 3). The F1 fault is the main fault that causes the Ayegan fault- propagation fold and the displacement at its tip-line reduce to zero, while the F_2 fault is extended during the folding. The occurrence of another fold in the backlimb of the Ayegan fold was already recognized (Fig.3); however, we consider both folds as parts of a fold train which formed above a thrust imbricate fan. In this study, we consider the most obvious fold as the reference FE-model for investigating the mechanical evolution of fault-propagation folds.

The FE-modelling was conducted in three main analysis steps. In the first step, a gravity load was applied to the entire model and the system was allowed to reach equilibrium. During the second step, an additional overburden pressure (= 50 MPa) was applied to the top of the study model to simulate a burial depth inferred for the time of deformation. The overburden pressure is defined as $P = \rho g h$; where ρ is the average density of overlying rocks (= 2500 kg/m^3), g is the gravitational acceleration (= 9.81 m/s^2), and h is the thickness (= 2045 m) or depth of the study model or example. One equilibrium conditions were achieved from the first two analysis steps, the deformation was imposed in a third step with folding and thrusting by a displacement 300 m along the hangingwall (hinterland or left side) to simulate contractional deformation.

During all analysis steps, the right side of the model (foreland) was restrained from horizontal movement (Ux=0) and the base of the model is constrained in all directions (Ux=Uy=0). The left side of the model, where gravitational load and overburden pressure are applied, was restrained from moving horizontally (Ux = 0) in the first and second steps, but it will move horizontally by 300 meters (U_x = 300m) in the third analysis step. It should be noted the F_1 fault tip is pinned in all three analysis steps (i.e., U_x=U_y=0), whereas the tip of fault F_2 is unrestrained. For all FE-model presented in this study, a friction coefficient of 0.01 was assigned to the fault interfaces. In addition, the friction coefficient of 0.25 was used for bedding interfaces. A total of 3969 triangular elements (2786 nodes) describe a model of 1300 × 345 m^2. The size of the model elements ranges from 14 to 50 meters.

Results

We present here the main features observed in the FE-models. Specially, we describe; 1) strain localization during the mechanical evolution of fault-propagation fold in a contractional environment, 2) the effect of mechanical properties, and overburden pressure on the fold geometry. Development and the evolution of deformation in the FE-models illustrate that mechanical properties and overburden pressure play an important role in fold geometries. To achieve these goals, we consider the following main results. The reference model results show that the slip is accommodated on thrust faults as they propagate up- and forward so that developed an open, asymmetric, and low-amplitude anticline at the tip of fault. As the deformation progresses, the fold amplitude, asymmetry, and lengthening with thinning in the forelimb increases due to the overall asymmetric anticline growth (Fig. 4). The development of minor discontinuities and also forelimb progressive rotation decreases the interlimb angle, i.e. the forelimb is steeper, which generally results in the steep or overturned forelimb and also with layer-parallel stretching. Hence, the forelimb and the fault zones in FE-models develops the largest strains (Fig. 4). Finally, a fault- propagation fold is formed that its half-wavelength and amplitude are 789 m 304 m, respectively (Fig.4).

Therefore, half-wavelength and amplitude in the reference model are larger than the natural model, and its forelimb and back- limb angles are equal to the natural model. However, its architecture is in harmony with natural fold architecture (Figs. 3, 4).

In the following sections, we construct and analyze a series of FE-models to test the effects of mechanical parameters and overburden pressure on the style of fault-propagation fold that develops.

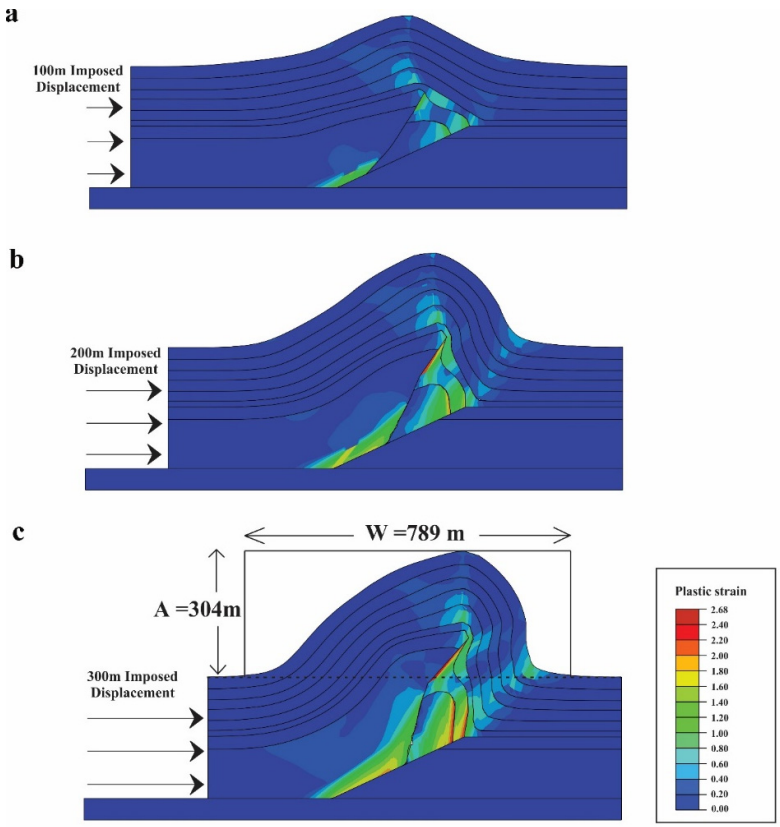

Figure 4. Observed structural geometry, internal deformation, and distribution of plastic strain of the fault-propagation fold after 100 m, 200 m, and 300 m of simulated thrusting. Half-wavelength and the amplitude of the fold structure are marked by 'W' and 'A', respectively

Effect of mechanical parameters

In order to evaluate the effects of different mechanical properties including Young's modulus, Poisson's ratio, dilation angle, and cohesion, in addition to the reference model, we also analyzed eight other models with a ±15% change in their values. (Fig. 5). Models with Young's modulus increased (Fig. 5a-I) and reduced (Fig. 5a-II) to 15% of the reference model values show final deformed geometries are characterized by lower overall half-wavelength magnitudes, 746 and 736 m, respectively, than the reference model (=789 m), although the shape of fault-propagation folds are generally similar to the reference model and including asymmetric geometries with a steep to overturned forelimb. The model with Young's modulus reduced to 15% lead to higher amplitude values (=305 m) with respect to both other models (Figs. 4 and 5a). In addition, models with the Poisson's ratio increased (Fig. 5b-I) and reduced (Fig. 5b-II) to 15% of the reference model values show final deformed geometries are characterized by lower overall half-wavelength magnitudes, 763 and 750 m, respectively, than the reference model (=789 m), although the shape of fault-propagation folds are generally similar to the reference model and including asymmetric geometries with a steep to overturned forelimb. Moreover, the model with the Poisson's ratio reduced to 15% lead to lower amplitude values (=301 m) with respect to both other models (Figs. 4 and 5a).

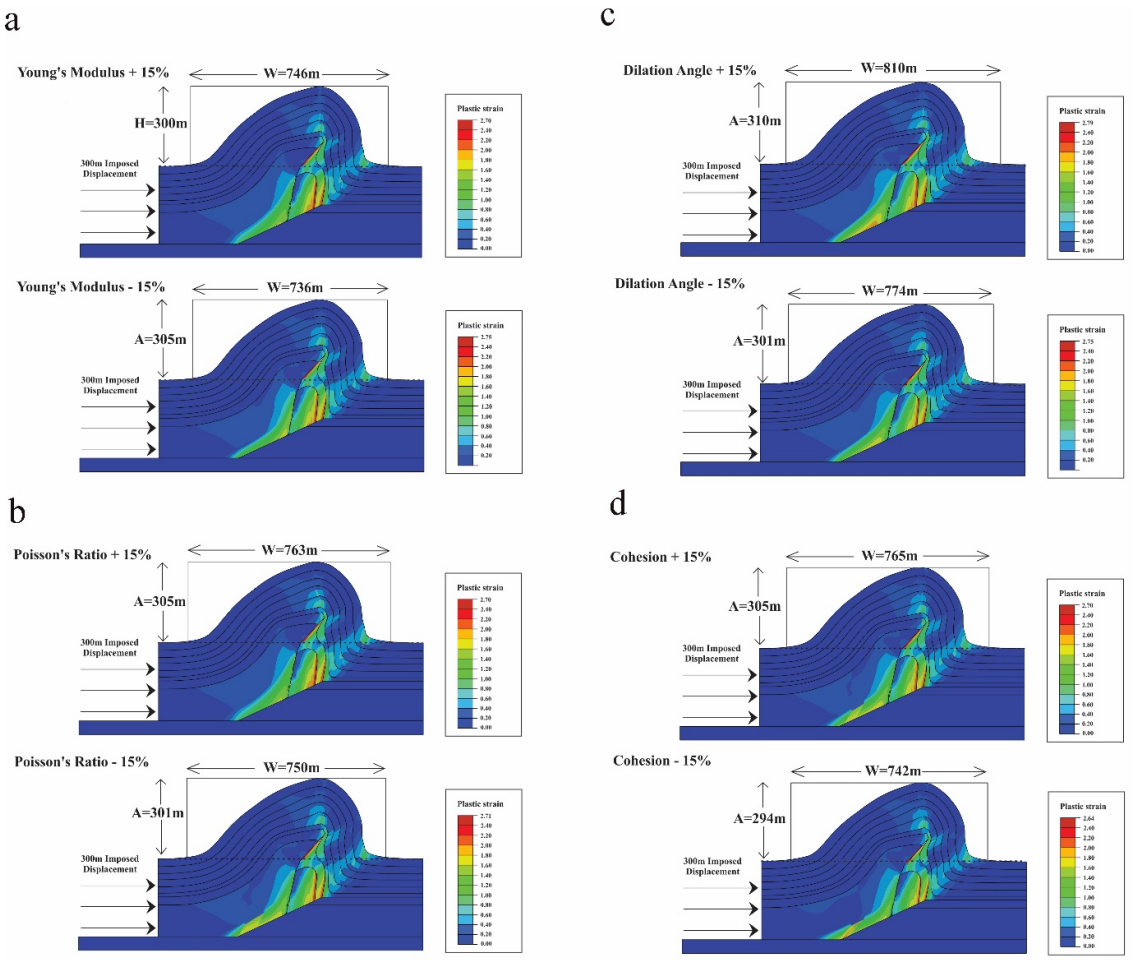

Figure 5. Structural style and magnitude of plastic strain for the FE-models of the fault-propagation folding for Young's modulus of +15% (a-I), -15% (a-II), Poisson's ratio of +15% (b-I), -15% (b-II), dilation angle of +15% (c-I), -15% (c-II), and the material cohesion of +15% (d-I), -15% (d-II) of the reference model. Half-wavelength and the amplitude of the fold structure are marked by 'W' and 'A', respectively

Models with the dilation angle increased (Fig. 5c-I) and reduced (Fig. 5c-II) to 15% of the reference model values show final deformed geometries are characterized by higher and lower overall half-wavelength magnitudes, 810 and 774 m, respectively, than the reference model (=789 m), although the shape of fault-propagation folds are generally similar to the reference model and including asymmetric geometries with a steep to overturned forelimb. The FE-modelling results show that the model with the dilation angle reduced to 15% lead to lower amplitude values (=301 m) with respect to other models (Figs. 4, 5a, 5b). Models with the material cohesion increased (Fig. 5d-I) and reduced (Fig. 5d-II) to 15% of the reference model values show final deformed geometries are characterized by lower overall half-wavelength magnitudes, 765 and 742 m, respectively, in both models than the reference model (=789 m), although the shape of fault-propagation folds are generally similar to the reference model and including asymmetric geometries with a steep to overturned forelimb. The model with the material cohesion reduced to 15% lead to lower amplitude values (=294 m) with respect to other models (Figs. 4, 5a, 5b, 5c).

Effect of overburden pressure

In order to evaluate the effects of the overburden pressure on the FE-model results, we considered two other FE-models with overburden pressures increased and decreased (Fig. 6a)) to 15% of the reference model values that show final deformed geometries, respectively, are characterized by lower the half-wavelength and the amplitude magnitudes (768 m and 302m, respectively), and higher the half-wavelength and the amplitude magnitudes (790 m and 306 m, respectively) with respect to the reference model (Fig. 6a). According to FE-model results, the dimensions of the fault-related folding are reduced in the higher overburden case (i.e., +15%) due to the increasing load required for deformation and material compaction, although the overall fold geometry and strain pattern are similar to the -15% overburden pressure and reference model, and vice versa. However, according to Fig. 6b, reduction in the overburden pressure condition led to somewhat greater displacement along the fault F1.

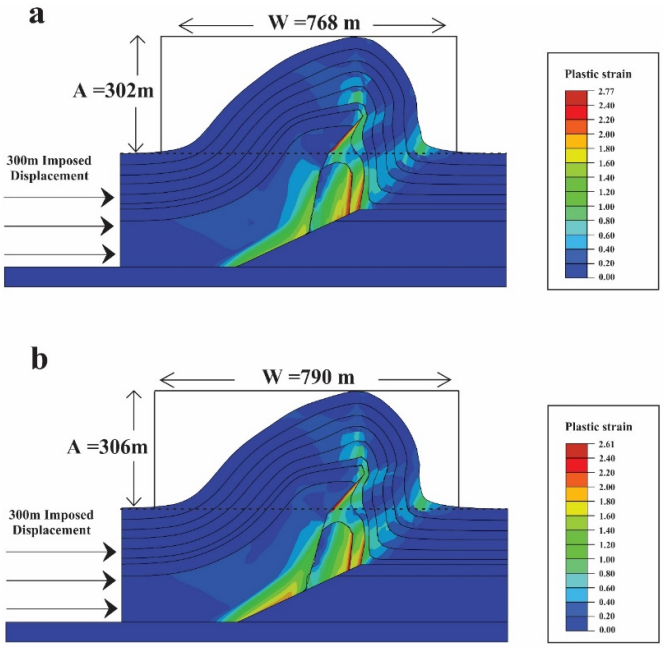

Figure 6. Structural style and magnitude of plastic strain for the FE-models of the fault-propagation folding for overburden pressure of +15% (a), and -15% (b) of the reference model. Half-wavelength and the amplitude of the fold structure are marked by 'W' and 'A', respectively

The effect of simultaneous mechanical parameters and overburden pressure

In order to evaluate the simultaneous effects of the overburden pressure and mechanical properties on the FE-model results, we considered two other FE-models with the increase in Young's modulus and overburden pressure, and with the decrease in Poisson's ratio, dilation angle, and cohesion simultaneously to 15% and 30%, respectively. The change in overburden pressures and mechanical properties to 15% (Fig. 7a) and 30% (Fig. 7b) of the reference model values show final deformed geometries, respectively, are characterized by lower overall half-wavelength (714 and 711 m) and lower amplitude (284 and 275 m) magnitudes with respect to the reference model (Fig. 4).

Discussion

The effect of material properties, mechanical stratigraphy, layer thickness, and other geomechanical parameter have been extensively investigated in many research (e.g., Chester, 2003; Cardozo et al., 2005; Ramsay & Huber, 2006; Hardy & Finch, 2007; Albertz & Sanz, 2012; Smart et al, 2012b; Feng & Gu, 2017; Bonano et al., 2017; Bulnes et al., 2018; Medina-Cascales et al., 2019). This study has considered some mechanical properties and boundary conditions that may be important factors in fault-related folding evolution. It has long been recognized that the structures that accommodate shortening within fold-and-thrust belts exhibit a wide variety of styles that reflect the mechanical behavior of the stratigraphic units that are being deformed. The ability to characterize these different structural styles, and to understand the factors that control their variability is important to many applications like regional tectonic studies.

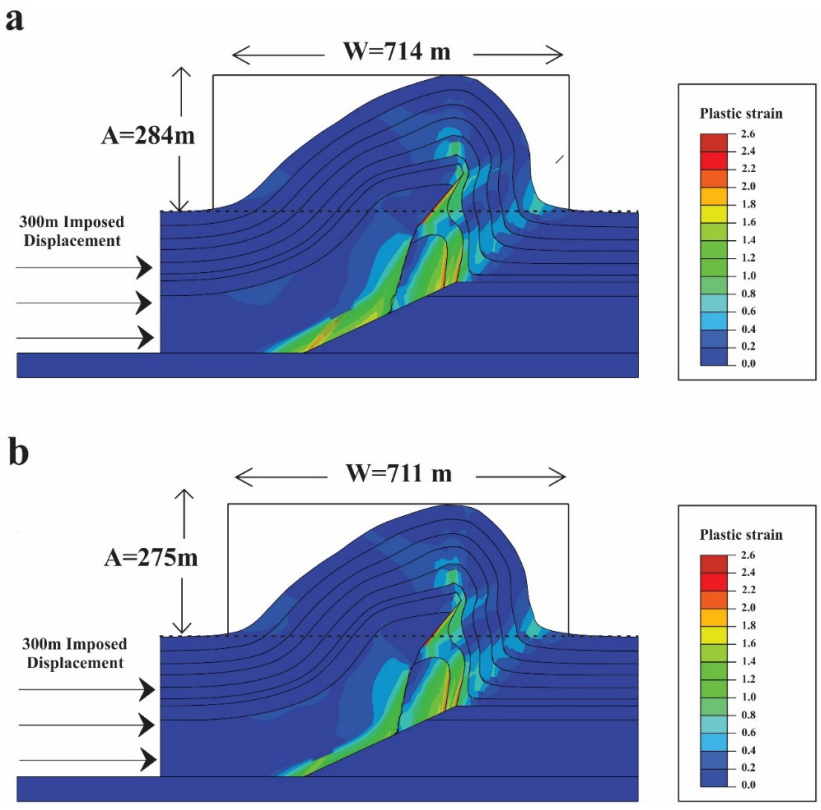

Figure 7. Structural style and magnitude of plastic strain for the FE-models of the fault-propagation folding for simultaneous mechanical parameters and overburden pressure of +15% (a), and +30% (b) of the reference model. Half-wavelength and the amplitude of the fold structure are marked by 'W' and 'A', respectively.

The relative contributions of different aspects of the mechanical stratigraphy and boundary conditions to studying fault-propagation folding style are investigated through the use of the 2D finite element models in this study. In this regard, where structural outcrops are lacking, covered and or where exposed lithologies are not suitable for standard and detail field-based observations or laboratory analysis techniques, FE-modelling provides a tool to complete and evaluate the mechanical evolution of the structure or sequences of them through the deformation history and strain localization.

In general, while 2D elastic-plastic FE-models in this study are an overall match to the Ayegan anticline geometry observed in the field, FE-model with the mechanical parameters and overburden pressure changed to 30% of the reference model show the most similarity and consistency in an overall sense and geometry with the natural example. The models replicate the overall asymmetry of the fault-propagation fold with a steeply dipping to overturned forelimb and the moderate to gently dipping backlimb so that at different time steps, the strain is localized in forelimb (characteristic of fault-propagation folding). The FE-modelling results in this study show that strain early in the folding and thrusting is marked by layer-parallel shortening and area loss (volume loss in 3D models), which in the natural structure of the Ayegan anticline could be manifest in the form of joints, pressure solution veins, and also fold-accommodation faults (Mitra, 2002a) including out-of-syncline thrust, into-anticline thrust, hinge wedge thrust, limb thrust, and forelimb thrust so that these secondary structures are common in nature and accommodate strain variation related to the structural and stratigraphic position during the evolution of folding and or fault-related folding. Area (and volume) loss can also lead to a decrease in permeability through intergranular mechanisms and the influence of mechanical properties (e.g. Young's modulus, Poisson's ratio, dilation angle, and cohesion) and overburden pressure. Hence, area and volume changes in fault-related folds (fault-propagation fold in this study) are as a function of mechanical stratigraphy, mechanical parameters, overburden pressure, pre-existing fault geometry, and structural positions. However, it should be noted that increasing strain especially in forelimb of the fault-related fold leads to increasing secondary fractures and faults frequency and permeability (e.g., Smart et al., 2010a, 2012b; Hughes et al., 2014).

Most of the fault -propagation folds are between trishear and kink-style kinematic models. These two models are the end members of fault-propagation folds deformation. Where lithology is heterogeneous, kink-style kinematic models dominate, and where lithology is homogenous, trishear models dominate (Hughes & Shaw, 2015). In this regard, according to the effect of heterogeneity resulting from mechanical stratigraphy in the Ayegan anticline, this structure is considered to be a kink-style kinematic model of the fault-propagation fold (e.g., Hughes & Shaw, 2015). Quantitative kink-style kinematic models of fault-propagation folding are based on two theories. They are the constant-thickness and fixed-axis theories; one based on conservation of layer thickness and bed length, and the other allowing thickening or thinning of beds in the forelimb (Suppe & Medwedeff, 1990). Therefore, only at the forelimb of the second theory, it is possible to change the area of the fold. While the results of our research showed that by changing the mechanical properties and boundary conditions (overburden Pressure), without changing in model stupe, fold's area is changed. This shows the importance of lithology and tectonic conditions in changing of fold area. Of course, pre-existing structures also play an important role in the strain localization during folding. In all models presented in this study, like the reference model, the strain localization is concentrated in the fault zones and the forelimb (Figs. 4- 8). Therefore, changing the mechanical properties do not play a significant role in the localization of the strain, and the effect of model setup (pre-existing faults) is probably more important.

Conclusions

We find that investigating a range of geometric and mechanical properties of fault-propagation

folds with a series of 2D finite-element elastic-plastic models in this study has helped to identify the mechanical (including Young's modulus, Poisson's ratio, dilation angle, cohesion) and boundary conditions (horizontal shortening with an additional overburden pressure) factors that are favorable and effective for the development of fault-propagation folds. Observation of the resulting structural geometries and strain localization over time steps of the mechanical evolution of FE-models provide insights into the effective factors, the position and style of deformation that is responsible for these observed changes. The FE-models suggest that overall fold width is established early and that as displacement increases along thrust faults the fold amplitude increases primarily by stretching and rotation of the forelimb. The forelimb region undergoes significant localized strain that would be expected to manifest as secondary faulting and fracturing in the natural structure. The FE-modelling results show models with the change in mechanical parameters and overburden pressure by 15% of the reference model values show final deformed geometries are characterized by different half-wavelength and amplitude magnitudes to the reference model although the shape of fault-propagation folds is generally similar to the reference model and including asymmetric geometries with a steep to overturned forelimb and thinning and thickening in the forelimb. Furthermore, all FE-models with the mechanical parameters reduced to 15%, except for Young's modulus overburden pressure, lead to lower half-wavelength and amplitude values with respect to the reference model. FE-model results show that area changes in fault-related folds (fault propagation fold in this study) are as function of mechanical stratigraphy, mechanical parameters, and overburden pressure and could be manifest in the form of joints, pressure solution veins, and also fold-accommodation faults in natural examples. Furthermore, this study shows that mechanical parameters and boundary conditions, in addition to the role of mechanical layering, can play important roles in the development of structural geometries of structures and affect the area of fold. Because fault-propagation folds are known as hydrocarbon reservoirs, therefore, variation in these parameters can affect the storage capacity of hydrocarbon resources. We apply these insights to the Ayegan anticline, central Alborz (as the natural contractional fault-propagation fold), that exhibit changes in structural style through mechanical evolution as a result of changes in mechanical parameters, overburden pressure, and fault performance and generally show well-designed FE-modelling can match overall structural geometry in the kink-style kinematic model.

Acknowledgments

The authors thank, Dr. Seyed Tohid Nabavi and Dr. Mohsen Ehteshami-Moinabadi for suggestions that improved this manuscript and Mr. Ali Hossein-Balam for training ABAQUS™ software. This article is part of the Ph. D thesis of Anis Khalifeh Soltani at Shahid Beheshti University.

References

Alavi, M., 1996. Tectonostratigraphic synthesis and structural style of the Alborz mountain system in northern Iran. Journal of Geodynamics, 21: 1 -33.

Albertz, M., Lingrey, S., 2012. Critical state finite element models of contractional fault-related folding: part 1. Mechanical analysis. Tectonophysics, 576-577: 133-149.

Albertz, M., Sanz, P.F., 2012. Critical state finite element models of contractional fault-related folding: part 2. Mechanical analysis. Tectonophysics, 576-577: 150-170.

Alipoor, R., Alavi., S. A., Abdollahie Fardc, I., Ghassemi, M. R., 2019. Structural analysis of the Aghajari and Pazanan anticlines, Dezful Embayment, SW Iran. Journal of Petroleum Science and Engineering, 176: 27-42.

Allen, M.B., Ghassemi, M.R., Shahrabi, M. and Qorashi, M., 2003. Accommodation of Late

Cenozoic oblique shortening in the Alborz Range, Northern Iran. Journal of Structural Geology, 25: 659- 672.

Ballato, P., Stockli, D.F., Ghassemi, M. R., Landgraf, A., Strecker, M.R., Hassanzadeh, J., Friedrich, A., and Tabatabaei, S.H., 2013. Accomodation of transpressional strain in the Arabia- Eurasia collision zone: new contraints from (UTh)/ He thermochronology in the Alborz Mountaions, N Iran. Tectonics, 32: 1- 18.

Ballato, P., Uba, C.E., Landgraf, A., Strecker, M.R., Sudo, M., Stockli, D.F., Friedrich, A. and Tabatabaei, S.H., 2011. Arabia-Eurasia continental collision: Insights from late Tertiary foreland basin evolution in the Alborz mountains, northern Iran. Geological Society of America Bulletin, 123: 106-131.

Bernard, S., Avouac, J.-P., Dominguez, S., Simoes, M., 2007. Kinematics of fault-related folding derived from sandbox experiments. J. Geophys. Res, 112: B03S12.

Bonanno, E., Bonini, L., Basili, R., Toscani, G., Seno, S., 2017. How do horizontal, frictional discontinuities affect reverse fault-propagation folding? Journal of Structural Geology, dio:10.1016/j.jsg.2017.08.001.

Brandes, C., Tanner, D.C., 2014. Fault-related folding: A review of kinematic models and their application. Earth-Science Reviews, 138: 352-370.

Bulnes, M., Poblet, J., Uzkeda, H., Rodríguez-álvarez, I., 2018. Mechanical stratigraphy influence on fault-related folds development: Insights from the Cantabrian Zone (NW Iberian Peninsula). Journal of Structural Geology, doi: 10.1016/j.jsg.2018.10.002.

Cardozo, N., Jackson, C.A.-L., Whipp, P.S., 2011. Determining the uniqueness of best-fit trishear models. J. Struct. Geol. 33, 1063-1078. Cardozo, N., 2005. Trishear modelling of fold bedding data along a topographic profile. J. Struct. Geol, 27: 495-502.

Chester, J., 2003. Mechanical stratigraphy and fault-fold interaction, Absaroka thrust sheet, Salt River Range, Wyoming. Journal of Structural Geology, 25: 1171-1192.

Cruz, L., Vásquez Serrano, A., Fitz-Díaz, E., Hudleston, P., 2019. Quantifying frictional variations and erosion in the Mexican fold-thrust belt. Journal of Structural Geology, 120: 1-13.

Derikvand, B., Alavi, S. A., Abdollahie Fard, I., Hajialibeigi, H., 2018. Folding style of the Dezful Embayment of Zagros Belt: Signatures of detachment horizons, deep-rooted faulting and syn-deformation deposition. Marine and Petroleum Geology, 91: 501-518.

Derikvand, B., Alavi, S. A., Abdollahie Fard, I., Jalali, L., 2019. Changing in fold geometry from faulted detachment fold to fault-bend fold, a case study: The Zeloi Anticline in the Dezful Embayment, southwest of Iran. Journal of Petroleum Science and Engineering, 173: 381-401

DeVecchio, D.E., Keller, E.A., Fuchs, M., Owen, L.A., 2012. Late Pleistocene structural evolution of the Camarillo fold belt: implications for lateral fault growth and seismic hazard in southern California. Lithosphere, 4: 91-109.

Ehteshami-Moinabadi, M. Yassaghi, A. 2013. Oblique inversion, a model for Oligocene-Miocene tectonics of south Central Alborz. Researches in Earth Sciences, 4: 32-50.

Ehteshami-Moinabadi, M. Yassaghi, A., 2007. Geometry and kinematics of the Mosha Fault, south central Alborz Range, Iran: An example of basement involved thrusting. Journal of Asian Earth Sciences, 29: 928-938.

Ehteshami-Moinabadi, M., Yassaghi, A. and Amini, A., 2012. Mesozoic basin inversion in Central Alborz, evidence from the Taleqan- Gajereh-Lar Paleograben. Journal of Geopersia, 2: 43-63.

Feng, J., Gu1, K., 2017. Geomechanical Modeling of Stress and Fracture Distribution during Contractional Fault-Related Folding. Journal of Geoscience and Environment Protection, 5: 61-93.

Ferrill, D.A., Morris, A.P., McGinnis, R.N., 2012. Extensional fault-propagation folding in

mechanically layered rocks: the case against the frictional drag mechanism. Tectonophysics, 576-577: 78-85.

Ghassemi, M. R., Fattahi, M., Landgraf, A., Ahmadi, M., Ballato, P., Tabatabaei, S. H., 2014. Kinematic links between the Eastern Mosha Fault and the North Tehran Fault, Alborz range, northern Iran. Tectonophysics, 622: 81- 95.

Guest, B., Axen, G.J., Lam, P.S. and Hassanzadeh, J., 2006b. Late Cenozoic shortening in the westcentral Alborz Mountain, northern Iran, by combined conjugate strike slip and thin-skinned deformation. Geosphere, 2: 35-52.

Guzofski, C.A., Shaw, J.H., Lin, G., Shearer, P.M., 2007. Seismically active wedge structure beneath the Coalinga anticline, San Joaquin basin, California. J. Geophys. Res, 112: B03S05.

Hardy, S., Finch, E., 2007. Mechanical stratigraphy and the transition from trishear to kink-band fault-propagation folds forms above blind basement thrust faults. A discrete-element study. Mar. Pet. Geol, 24: 75-90.

Hughes, A.N. and Shaw, J.H., 2015. Insights into the mechanics of fault-propagation folding styles. GSA Bulletin, 127(11-12):1752-1765.

Hughes, A.N., Benesh, N.P. and Shaw, J.H., 2014. Factors that control the development of fault-bend versus fault-propagation folds: Insights from mechanical models based on the discrete element method (DEM). Journal of Structural Geology, 68: 121-14.

Jabbour, M., Dhont, D., Hervouët, Y., Deroin, J. P., 2012. Geometry and kinematics of fault-propagation folds with variable interlimb angle. Journal of Structural Geology, 42: 212- 226.

Johnson, K.M., Segall, P., 2004. Imaging the ramp-décollement geometry of the Chelungpu fault using coseismic GPS displacements from the 1999 Chi-Chi, Taiwan earthquake. Tectonophysics, 378: 123-139.

Landgraf, A., Ballato, P., Strecker, M. R., Friedrich, A., Tabatabaei, S. H., and Shahpasandzadeh, M., 2009. Fault-kinematic and geomorphic observations along the North Tehran Thrust and Mosha-Fasham Fault, Alborz Mountains, Iran: Implications for fault-system evolution and interaction in a changing tectonic regime, Geophys. J. Int., 177: 676-690, doi:10.1111/j.1365-246X.2009.04089.x.

Lin, M.L.,Wang, C.P., Chen,W.S., Yang, C.N., Jeng, F.S., 2007. Inference of trishear-faulting processes fromdeformed pregrowth and growth strata. J. Struct. Geol, 29: 1267-1280.

Maerten F., Maerten L., Pollard D.D., 2014. iBem3D, a three-dimensional iterative boundary element method using angular dislocations for modeling geologic structures. Computers & Geosciences, 72: 1-17.

McClay, K.R., 1995. The geometries and kinematics of inverted fault systems: a review of analogue model studies. In: Buchanan, J.G., Buchanan, P.G. (Eds.), Basin InversionGeol. Soc. Spec. Publ, 88: 97-118 (London).

Medina-Cascales, I., Koch, L., Cardozo, N., Martin-RojasI., Alfaro, P., García-Tortosa, F. J., 2019. 3D geometry and architecture of a normal fault zone in poorly lithified sediments: A trench study on a strand of the Baza Fault, central Betic Cordillera, south Spain. Journal of Structural Geology https://doi.org/10.1016/j.jsg.2019.02.003.

Mitra, S., 1990. Fault-propagation folds: geometry, kinematic evolution, and hydrocarbon traps. AAPG Bull, 74: 921-945.

Mitra, S., 2002a. Fold-accommodation faults. AAPG Bull, 86: 671-693.

Nabavi, S. T., Alavi, S. A., Díaz-Azpiroz, M., Mohammadi, S., Ghassemi, M.R., Fernandez, C., Barcos, L., Frehner, M., 2020. Deformation mechanics in inclined, brittle-ductile transpression zones: Insights from 3D finite element modelling. Journal of Structural Geology, 137: 104082.

Nabavi, S. T., Alavi, S. A., Maerten., F., 2018b. 2D finite-element elastic models of transtensional pull-apart basins. Comptes Rendus Geoscience, 350: 222-230.

Nabavi, S. T., Alavi, S. A., Mohammadi, S., Ghassemi, M.R., 2018a. Mechanical evolution of

transpression zones affected by fault interactions: Insights from 3D elasto-plastic finite element models. Journal of Structural Geology, 106: 19-40.

Nabavi, S. T., Alavi, S. A., Mohammadi, S., Ghassemi, M.R., Frehner, M., 2017b. Analysis of transpression within contractional fault steps using finite-element method. Journal of Structural Geology, 96: 1-20.

Nabavi, S.T., Díaz-Azpiroz, M., Talbot, C.J., 2017a. Inclined transpression in the Neka Valley, eastern Alborz, Iran. International Journal of Earth Sciences, 106: 1815-1840.

Ramsay J, Huber M, 1987. The techniques of modern structural geology, Fold and fractures. Academic Press, London, 2: 1- 462.

Smart, K.J., Ferrill, D.A., Morris, A.P., McGinnis, R.N., 2012b. Geomechanical modelling of stress and strain evolution during contractional fault-related folding. Tectonophysics, 576-577: 171-196.

Stocklin, J., 1968. Structural History and Tectonic of Iran: A Review. American Association of Petroleum Geologists Bulletin, USA, 52: 1229-1258.

Suppe, J., 1983. Geometry and kinematics of fault-bend folding. Am. J. Sci, 283: 684-721.

Suppe, J., Medwedeff, D.A., 1990. Geometry and kinematics of fault-propagation folding. Eclogae Geol. Helv, 83: 409-454.

Thebian, L., Najjar, S., Sadek, S., Mabsout, M., 2017. Numerical investigation of dip-slip fault propagation effects on offshore seabed sediments. Engineering Geology, 237: 149- 167.

Vahdati- Daneshmand, F., 2001. Geological map of Marzan- Abad, Iran. Geological survey of Iran, Scale 1: 100,000.

Vernant, P., Nilforoushan, F., Hatzfeld, D., Abbassi, M., Vigny, C., Masson, F., Nankali, H., Martinod, J., Ashtiani, M., Bayer, R., Tavakoli, F., and Chéry, J., 2004. Present-day crustal deformation and plate kinematics in the Middle East constrained by GPS measurements in Iran and northern Oman. Geophys. J. Int, 157: 381- 398.

Williams, G., Chapman, T., 1983. Strains developed in the hangingwalls of thrusts due to their slip/propagation rate: a dislocation model. J. Struct. Geol, 5: 563-571.

Yassaghi, A. and Madanipour, S., 2008. Influence of a transverse basement fault on along-strike variations in the geometry of an inverted normal fault: Case study of the Mosha Fault, Central Alborz Range, Iran. Journal of Structural Geology, 30: 1507-1519.

Yassaghi, A., Naeimi, A., 2011. Structural analysis of the Gachsar sub-zone in central Alborz range; constrain for inversion tectonics followed by the range transverse faulting. International journal of earth sciences, 100: 1237-1249.

Zanchi, A., Zanchetta, S., Berra, F., Mattei, M., Garzanti, E., Molyneux, S., Nawab, A., Sabouri, J., 2009. The EoCimmerian (Late? Triassic) orogeny in north Iran. In: Brunet, M.F., Wilmsen, M., Granath, J.W. (Eds.), South Caspian to Central Iran Basins. Geological Society, London, Special Publications, 312: 31-55.